The Astrophysical Journal Letters, 883:L10 (7pp), 2019 September 20 https://doi.org/10.3847/2041-8213/ab3f2f

Suprathermal Ion Abundance Variations in Corotating Interaction Regions over Two Solar Cycles

Robert C. Allen, George C. Ho, and Glenn M. Mason
Johns Hopkins Applied Physics Laboratory, 11100 Johns Hopkins Road, Laurel, MD 20723-0452, USA; Robert.Allen@jhuapl.edu
Received 2019 April 24; revised 2019 August 27; accepted 2019 August 28; published 2019 September 18

Abstract

Suprathermal ion composition associated with corotating interaction regions (CIRs) exhibited a solar cycle variation during solar cycle 23 and the beginning of solar cycle 24. However, it is unclear if this variation would remain when considering all of solar cycle 24, or whether the variations in the CIR-associated suprathermal ion composition would change. Using 20 yr of *Advanced Composition Explorer* observations (1998–2018), we present a comparison of the suprathermal ion compositions for solar cycles 23 and 24. The energetic particle content for the two solar cycles is found to be remarkably similar. The observed solar cycle variations in 0.32–0.45 MeV/nuc Fe/O previously observed for solar cycle 23 was seen to be largely repeated in solar cycle 24, both in solar cycle phase and magnitude. A small enhancement in CIR-associated Fe/O during the declining phase was observed for both solar cycles. The CIR event-averaged intensities of Fe and O were also found to have a slight solar cycle dependence, with the Fe/O ratio being more closely bound to the intensity of Fe ions. Additionally, the elemental abundance versus O ratios compared to the Fe/C ratios were found to follow the same trends for both solar cycles, with high Fe/C ratio events occurring mostly during solar maximum.

Key words: acceleration of particles – solar wind – Sun: abundances – Sun: heliosphere

1. Introduction

Corotating interaction regions (CIRs) are major sources of energetic particles in the interplanetary medium (e.g., Van Hollebeke et al. 1981; Tsurutani et al. 1982; Richardson 2018). CIRs arise when fast solar wind streams from coronal holes overtake slower solar wind. Shocks, which can accelerate particles, may form at the leading and trailing edge of the CIR at, or more often beyond, 1 au (e.g., Smith & Wolfe 1976; Richardson 2018). Additionally, CIRs have been shown to trigger geomagnetic storms (e.g., Tsurutani & Gonzalez 1997; Richardson et al. 2006; Turner et al. 2006; Richardson 2018), as well as affect ionosphere/thermosphere densities, winds, and compositions (e.g., Chen et al. 2014).

While the composition of energetic particles associated with CIRs is generally similar to the composition of the bulk solar wind, there are important differences. For example, CIRs are often observed to have He^{+} and ^{3}He abundances enhanced well above those observed in the bulk solar wind (e.g., Gloeckler et al. 1994a; Möbius et al. 2002). These compositional differences suggest the seed population for energetic CIR particles are from both the heated bulk solar wind and the suprathermal ion pool (e.g., suprathermal solar wind, pick-up ions, accelerated ^{3}He particles accelerated by flares, shocked plasma, stochastically accelerated particles, energetic neutral atoms from the heliosheath, and ions from Sun-grazing comets; see Mewaldt et al. 2012), although this remains an open area of research (e.g., Gloeckler et al. 1994a; Mason 2000; Möbius et al. 2002; Mason et al. 2008, 2012; Filwett et al. 2017).

CIR-associated energetic particles have also been observed to have a compositional solar cycle variation (e.g., Mason et al. 2008, 2012; Filwett et al. 2017). Mason et al. (2012) observed a Fe/O variation over the course of solar cycle 23 in a sample of CIRs from 1998 to 2011. They found a fairly high correlation (correlation coefficient of 0.695) between the CIR-associated 0.32–0.45 MeV/nuc Fe/O and the mean sunspot number. This strong correlation was interpreted as suggesting Fe/O was possibly affected by the quiet-time (devoid of dynamic changes in solar wind such as shocks or flare events) suprathermal heavy ion (heavier than H) abundances, which are known to have a relationship with sunspot number (e.g., Desai et al. 2006; Dayeh et al. 2009). However, Mason et al. (2008) did note that observed deviations in Fe/O from the sunspot number were also suggestive of other processes being at play. This study expands upon previous work by extending the CIR list to include nearly all of solar cycle 24 in order to examine the properties of CIR-associated suprathermal ion composition over two solar cycles. Doing so allows us to determine if the observed compositional solar cycle variations observed during CIR events are continued for solar cycle 24, which will help determine if these variations are, in fact, correlated with solar cycle phase and help predict CIR-associated abundances in future solar cycles as well as aid in the interpretation of measurements by *Parker Solar Probe* and *Solar Orbiter*.

2. Observations

The *Advanced Composition Explorer* (*ACE*) spacecraft has been orbiting the sunward Lagrangian point (L1) since 1997. This study uses observations from the Ultra-Low Energy Isotope Spectrometer (ULEIS; Mason et al. 1998) on board *ACE* to study the CIR-associated suprathermal ion abundances over the course of nearly two solar cycles (observations: 1998–2018 for cycles 23 and 24). In order to study possible similarities and differences between the two cycles, we extended the ULEIS CIR lists from cycle 23 (Mason et al. 2008) and the first part of 24 (Mason et al. 2012) through the end of 2018 (nearly the end of cycle 24). This was done using the same event selection criteria stated in Mason et al. (2008): (1) increase in solar wind flow speed; (2) increase in density just upstream of the interface; (3) increase in magnetic field magnitude just upstream of the interface; (4) dispersionless increase in energetic particle intensity lasting at least 24 hr; (5) 230–320 keV/nuc He

intensity exceeding 10 $(s^{-1}\,cm^2\,sr\,MeV/nuc)^{-1}$; and (6) during times without other sources of solar energetic particles (SEP; see Mason et al. 2008 for additional details). The full list is provided in Table 1. Columns 2–4 list the start year, day of year (DOY), and duration of periods when the O intensities were well above background levels, following the methodology of Mason et al. (2012). Only a subset of CIRs meet the stringent criteria for event selection needed to study the suprathermal ion composition variations.

Figure 1(A) illustrates the suprathermal (0.32–0.45 MeV/nuc) Fe/O ratios (blue diamonds), using a three-event running average, along with the monthly (black lines) and smoothed (red lines) sunspot numbers, as done in Mason et al. (2012). The Fe/O correlation with sunspot number observed during solar cycle 23 (Mason et al. 2012) is found to persist during cycle 24. The Pearson correlation coefficient between sunspot number and Fe/O for 1998–2018 is found to be 0.652, less than a 0.01% chance of being exceeded by uncorrelated quantities. Mason et al. (2012) interpreted the scaled Fe/O distribution during the ascending phase of cycle 23 as "lagging" the sunspot numbers before becoming more in phase with sunspot number during solar maximum. However, a similar lag is not seen during the ascending phase of cycle 24. Expanding the study to both solar cycles shows that Fe/O is roughly in phase with the sunspot number beyond the solar maximum of cycle 23 (after 2000) with enhancements in the declining phase of both solar cycles (i.e., 2005–2006 and 2017–2018).

To investigate any solar cycle dependence of the event-averaged Fe and O intensities, both quantities are plotted versus sunspot number in Figure 1(B). The O intensities (magenta diamonds) are divided by 10 to show alongside the Fe intensities (blue diamonds). A solar cycle dependence is observed for both species (Figure 1(B)), although the intensities have more variability than their ratio. The O and Fe intensities have Pearson correlation coefficients to the sunspot number of 0.4560 and 0.5196, respectfully, both a <0.01% chance of being exceeded by uncorrelated quantities. Figures 1(C) and (D) illustrate the Fe/O ratio versus the O and Fe intensities, respectively, for cycles 23 (purple triangles) and 24 (green diamonds) along with a power-law fit. The correlation coefficient of the Fe/O ratio versus O and Fe intensities to the power-law fits are 0.7828 and 0.7724, respectively. While a correlation between the Fe/O ratio and either intensity is observed (i.e., higher-intensity events have a higher Fe/O ratio), the variance of Fe/O versus O is higher than versus Fe. Additionally, the slope for the CIR-associated Fe/O ratio versus O intensity is lower than versus the Fe intensities.

The average suprathermal elemental abundance normalized to O for all CIRs in both solar cycles is illustrated in Figure 2 along with the average bulk solar wind abundance for slow and fast streams. Average CIR relative ion abundances for all species are nearly identical during both solar cycles. As previously noted (Mason et al. 2008), with the exception of He and Ne, the relative abundances of CIR-associated suprathermal ions are similar to the solar wind abundances, particularly for the fast solar wind (e.g., Ca). However, compared to both fast and slow solar wind, the CIR-associated abundances of He and Ne are significantly enhanced for both solar cycles.

To investigate the relative event-to-event abundance variations, event-averaged abundances are shown in Figure 3 for each species relative to O versus the Fe/C ratio for that event. The left column of Figure 3 shows the events separated by solar cycle. Fitting the points with a power law results in nearly

Table 1
Corotating Interaction Region Events from 1998 to 2018

Event	Start Year	Start DOY	Length (days)
(1)	(2)	(3)	(4)
1[a]	1998	197.25	2.00
2[a]	1998	204.00	1.50
3[a]	1999	60.75	1.75
4[a]	1999	138.25	1.50
5[a]	1999	228.25	1.50
6[a]	1999	284.50	1.75
7[a]	1999	311.25	1.25
8[a]	1999	338.00	1.25
9[a]	1999	364.75	3.00
10[a]	2000	27.50	1.25
11[a]	2000	37.25	2.00
12[a]	2000	55.00	2.25
13[a]	2000	82.50	2.00
14[a]	2000	342.25	3.25
15[a]	2002	89.75	3.25
16[a]	2002	325.50	1.50
17[a]	2003	46.50	2.00
18[a]	2003	207.75	1.25
19[a]	2003	233.50	2.00
20[a]	2003	260.00	2.50
21[a]	2003	314.25	1.50
22[a]	2003	318.50	3.00
23[a]	2004	43.25	1.50
24[a]	2004	325.60	1.40
25[a]	2005	65.50	2.00
26[a]	2005	281.00	1.50
27[a]	2005	334.00	3.00
28[a]	2005	361.50	1.25
29[a]	2006	99.25	1.50
30[a]	2006	212.50	2.00
31[a]	2006	219.25	2.25
32[a]	2006	239.75	1.75
33[a]	2006	267.00	1.25
34[a]	2006	293.50	2.50
35[a]	2007	1.75	2.75
36[a]	2007	29.50	1.40
37[a]	2007	44.50	3.50
38[a]	2007	58.75	1.75
39[a]	2007	71.75	3.25
40[a]	2007	127.75	2.00
41[a]	2007	138.25	1.25
42[b]	2007	192.00	3.00
43[b]	2007	264.50	2.00
44[b]	2007	298.50	1.50
45[b]	2007	324.50	2.50
46[b]	2007	351.50	3.00
47[b]	2008	5.25	3.25
48[b]	2008	41.25	3.25
49[b]	2008	222.25	2.75
50[b]	2008	275.25	2.75
51[b]	2008	330.00	3.00
52[b]	2009	175.50	3.50
53[b]	2009	191.00	2.50
54[b]	2010	122.50	2.50
55[b]	2010	150.75	3.75
56[b]	2010	236.00	3.50
57[b]	2010	295.25	1.50
58[b]	2011	35.75	1.75
59[b]	2011	60.00	5.50
60[b]	2011	120.00	2.75
61[b]	2011	173.75	3.25
62	2011	362.25	2.00
63	2012	144.00	2.00

Table 1
(Continued)

Event	Start Year	Start DOY	Length (days)
(1)	(2)	(3)	(4)
64	2012	182.25	1.75
65	2012	231.50	1.00
66	2013	152.25	1.50
67	2013	171.75	1.00
68	2013	281.50	1.00
69	2014	50.50	2.00
70	2014	83.50	2.00
71	2014	340.75	1.50
72	2015	159.00	2.00
73	2015	192.25	1.00
74	2015	307.25	1.00
75	2016	216.25	2.00
76	2016	327.75	1.50
77	2016	343.25	1.25
78	2017	31.25	1.50
79	2017	80.75	1.25
80	2017	82.75	1.00
81	2017	96.00	1.00
82	2017	111.50	3.00
83	2017	140.25	1.00
84	2017	216.25	1.25
85	2017	244.50	1.50
86	2017	339.25	1.25
87	2018	110.50	2.00

Notes.
[a] CIR intervals from Mason et al. (2008).
[b] CIR intervals from Mason et al. (2012).

identical fits, within reasonable error, for both solar cycles showing the same correlations as observed for cycle 23 by Mason et al. (2008). While cycle 24 observed several CIRs with higher Fe/C than observed in cycle 23, the points generally still follow the fitted power laws.

Also as noted in Mason et al. (2008), He/O, and to a lesser degree Ne/O, ratios show a downward slope with respect to Fe/C. This cannot by explained by variations of solar wind composition between fast and slow streams. The relative abundances of C and O are similar between slow and fast wind, and since the Fe, He, and Ne are more abundant in the slow than the fast solar wind, this would lead to a positive correlation (von Steiger et al. 2000). However, it is possible that the variations along the power-law slopes are, at least partially, due to a solar cycle effect on the solar wind composition, with the He/O ratios and Ne/O ratios varying throughout the solar cycle (see Desai et al. 2006; Mason et al. 2008). In order to investigate solar cycle phase dependencies in the abundance ratios, the right column of Figure 3 illustrates the ratios by solar cycle phase. To define the phase, the smoothed sunspot number was normalized to the maximum for each solar cycle and broken up into times when the normalized sunspot number was less than 1/3 (solar minimum, blue triangles), greater than 2/3 (solar maximum, red diamonds), or in between (ascending/descending phase, green rectangles). As would be expected from the Fe/O ratio in Figure 1, all of the times the Fe/C ratios were greater than approximately 0.3 occurred during solar maximum. However, the ratios during solar minimum and the declining/ascending phase are very similar. While the solar maximum Fe/C ratios extend to much higher values than for CIRs during either solar minimum or the declining/ascending phases, some of the solar maximum CIRs are also observed to have Fe/C ratios well within the range of values observed for the other phases. This seems to suggest that the process(es) that is/are energizing Fe preferential to C can be more efficient during solar maximum, but the process(es) does/do not require all CIR-associated Fe/C ratios during solar maximum to be necessarily elevated above that during the other phases. An example of this is the Fe/O enhancement during the declining phase (Figure 1).

3. Discussion

This study extends the studies of Mason et al. (2008, 2012) to include both cycles 23 and 24 (1998–2018). CIR-associated suprathermal ion abundances in cycle 24 are found to be remarkably similar to those in cycle 23. There was virtually no change in the ion abundances between the two cycles when averaging over all CIR intervals within each solar cycle, finding abundances relative to O are similar to fast solar wind abundances with the exception of He and Ne (see Figure 2). Additionally, the elemental abundances of suprathermal ions relative to O follow the same power-law slopes versus Fe/C as cycle 23 (see Figure 3). One of the few differences between the solar cycles is that cycle 23 had an observed lower Fe/O ratio versus sunspot number during the ascending phase (see Mason et al. 2012); however, Fe/O and sunspot number are in phase and largely above that of the sunspot number scaled by 0.001 for the entirety of cycle 24 (see Figure 1(A)).

These results are consistent with CIR-associated suprathermal ions being from both heated solar wind ions and from an additional suprathermal ion pool, as suggested in previous studies (e.g., Mason et al. 2008, 2012; Filwett et al. 2017). This can be most easily seen in Figure 2 in that the CIR-associated abundances of He and Ne differ from the bulk solar wind composition, thereby necessitating some additional source. It is likely that the bulk solar wind is energized through some process into the suprathermal ion energy range before mixing with preexisting suprathermal ions (see Mason et al. 2012). Supporting this part of the two-step energization pathway, work has previously been done to correlate the composition of CIR-associated suprathermal particles with upstream thermal solar wind ions and found that the CIR-associated suprathermal population correlated well with solar wind 4 days before the CIR (Mason et al. 2008; Filwett et al. 2017). It is possible that SEPs or flare-associated suprathermal particles could have been entrained in the population along a CIR-associated shock at further distances. In this particular scenario, these accelerated ions can propagate along field lines toward the Sun (and *ACE*; e.g., Roelof 2000). This is consistent with the interpretation of previous studies (e.g., Marshall & Stone 1978; Richardson 1985; Mason et al. 2008, 2012; Ebert et al. 2012; Filwett et al. 2017). He and Ne have the highest first ionizing potential (FIP) of the species shown (Figure 2), which could suggest that pick-up ions are being accelerated within the CIR (e.g., Glockler et al. 1994b; Schwadron et al. 1996).

Correlating the Fe/O ratio to the event-averaged intensity of Fe and O provides notable insights into the acceleration mechanism of energetic particles during CIRs (Figure 1). The CIR-associated Fe/O ratio versus O intensity is found to be correlated with a lower slope and higher variability than versus the Fe intensity. This may suggest preferential acceleration of

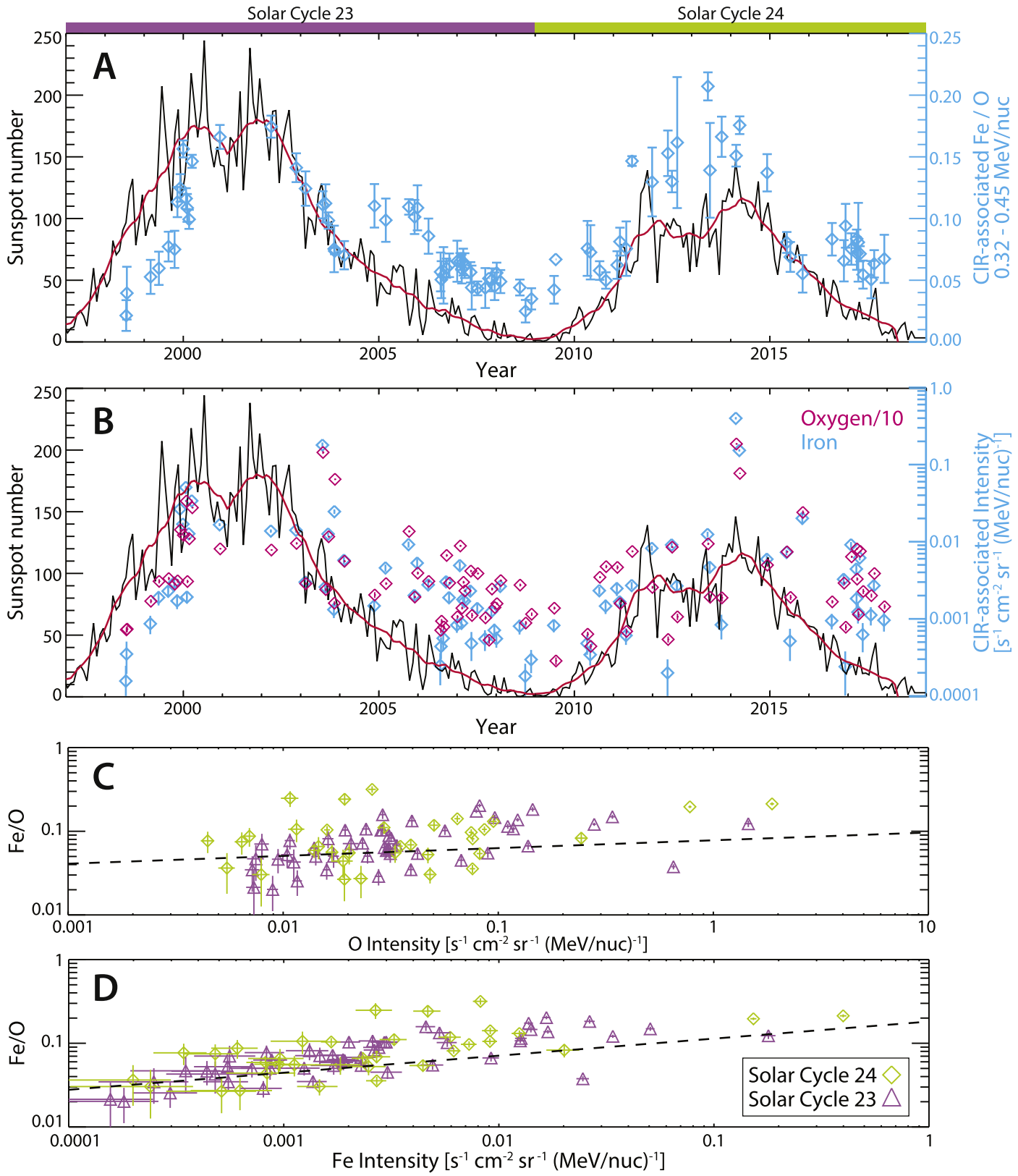

Figure 1. (A) Event-averaged CIR-associated 0.32–0.45 MeV/nuc Fe/O (blue) smoothed over three events, along with the mean monthly sunspot number and smoothed sunspot number (black and red lines, respectively). The purple and green bars (top) denote the intervals for solar cycles 23 and 24, respectively. (B) Event-averaged Fe (blue) and O (magenta, divided by 10) intensities are shown against the sunspot trends. Fe/O ratios vs. the event-averaged O intensity (C) and Fe intensity (D) are shown for solar cycles 23 (purple) and 24 (green) along with a power-law fit (dashed line).

Fe than O taking place during solar maximum. This could suggest that one of the processes affecting CIR-associated suprathermal particle composition tied to the solar cycle phase accelerates ions by either a mass/charge (Drake et al. 2009; Li & Lee 2015; Zhao et al. 2016, 2017) or FIP dependence (Feldman & Widing 2002), leading to more Fe than O ions

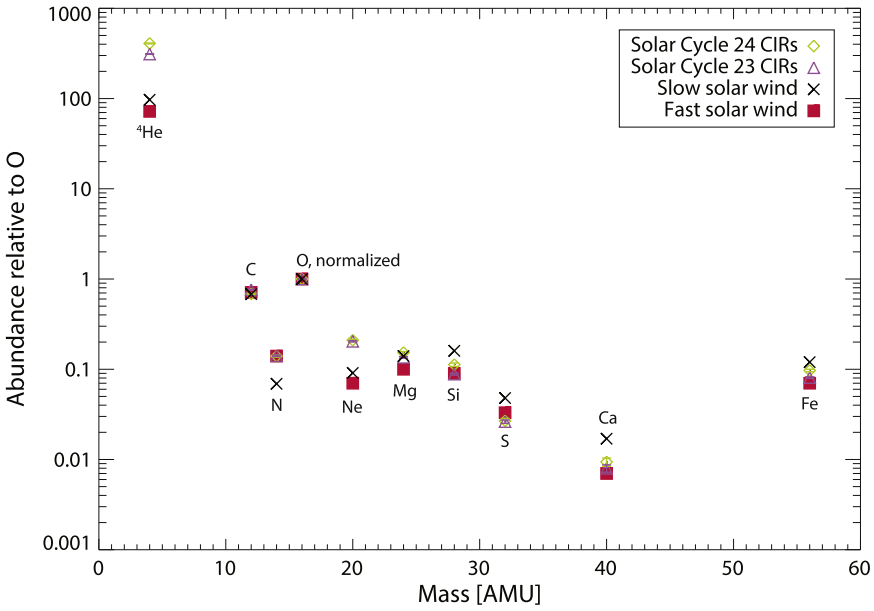

Figure 2. Average CIR-associated 0.32–0.45 MeV/nuc abundances normalized to O for cycles 23 (purple triangles) and 24 (green diamonds) compared to the average relative solar wind abundances for slow (black crosses) and fast (red squares) streams (von Steiger et al. 2000; Wurz et al. 2003; Gloeckler & Geiss 2007).

being energized into the suprathermal energy range. Comparing the slopes of the relative event-averaged composition (Figure 3) reveals that the slope increased with M/q for species with positive slopes (Mg, Si, S, Ca, and Fe listed in order of M/q). It should be noted that both He and Ne, the two species with abundances higher than that found in fast streams, have negative slopes, while N, which is found to have a slope near 0, is extremely consistent in relative abundance with the fast wind (Figure 2). This could suggest an M/q acceleration for ions in the bulk solar wind, and that the preexisting suprathermal pool largely consists of Ne, N, and He. These three species are also the highest FIP species investigated in this study, which could indicate that interstellar pick-up ions are a significant seed population for CIR-associated suprathermal particles (e.g., Glockler et al. 1994b; Schwadron et al. 1996).

The results of this study indicate that the processes populating the suprathermal ion energy range during CIR events have repeatable solar cycle variations. The fact that the CIR-associated suprathermal Fe/O ratio during cycle 24 matched, and in some cases exceeded, that of cycle 23 (see Figure 3), despite the maximum sunspot number being lower in cycle 24, would seem to indicate that the solar cycle phase dependence of the composition is not directly tied to the magnitude of solar activity from one solar cycle to the next (as illustrated by the sunspot number). The enhancements of the Fe/O observed in the declining phase, but not the ascending phase, of both cycles 23 and 24 may also point to repeatable processes that are not directly linked to solar activity as evidenced by sunspot number. Rather, both solar activity and CIR suprathermal ion composition are likely both mutually correlated to some other process or processes, and the seed populations may differ between ascending and descending phases of the solar cycle.

The similarities between cycles 23 and 24 for the CIR-associated ion composition distinguishes CIRs from the compositional variability seen in SEP events. Previous work investigating SEP fluences and composition during both cycle 23 and the first 5.8 yr of cycle 24 found that the SEP fluences were notably lower during the start of solar cycle 24 and that the ratios of fluence between cycles 23 and 24 by species follow a power law versus the species charge-to-mass ratio (Mewaldt et al. 2015). Mewaldt et al. (2015) concluded that the reduction in SEP production during solar cycle 24 could be due to a combination of a lower magnetic field strength in interplanetary space and a reduction in seed particle densities. The lower interplanetary magnetic field strength could act to limit the efficiency of accelerating particles up to SEP energy ranges (e.g., see Gopalswamy et al. 2014; Mewaldt et al. 2015). Meanwhile, the lower seed particle densities would act to limit the maximum energies particles could be accelerated by Alfvén waves at a shock front through nonlinear interactions (e.g., Li et al. 2005). This then raises the question if CIR-associated intensities are similarly modulated by the interplanetary magnetic field strength and suprathermal ion seed populations. Unlike for SEPs, the event-averaged intensity ratios were found to be the same for cycles 23 and 24 (Figure 3), despite the weaker interplanetary magnetic field. Instead, the similarities between the CIR-associated plasma would seem to suggest that the processes leading to the observed solar cycle variations in the abundance ratios would need to be occurring in the same fashion between the two solar cycles, unlike for the SEP-related processes.

One notable feature that will be the topic of future investigations is the small enhancement of CIR-associated Fe/O during the declining phase of both solar cycles. This feature could provide needed clues into the mechanism that is heating ions into the suprathermal ion pool as well as possible variations in the composition and/or abundance of seed particle populations and merits an in-depth analysis beyond the scope of this Letter. Another avenue of future work will be to investigate possible correlations between the solar cycle dependence to other quantities that vary during the solar cycle, particularly those that may influence the suprathermal ion pool and ion energization.

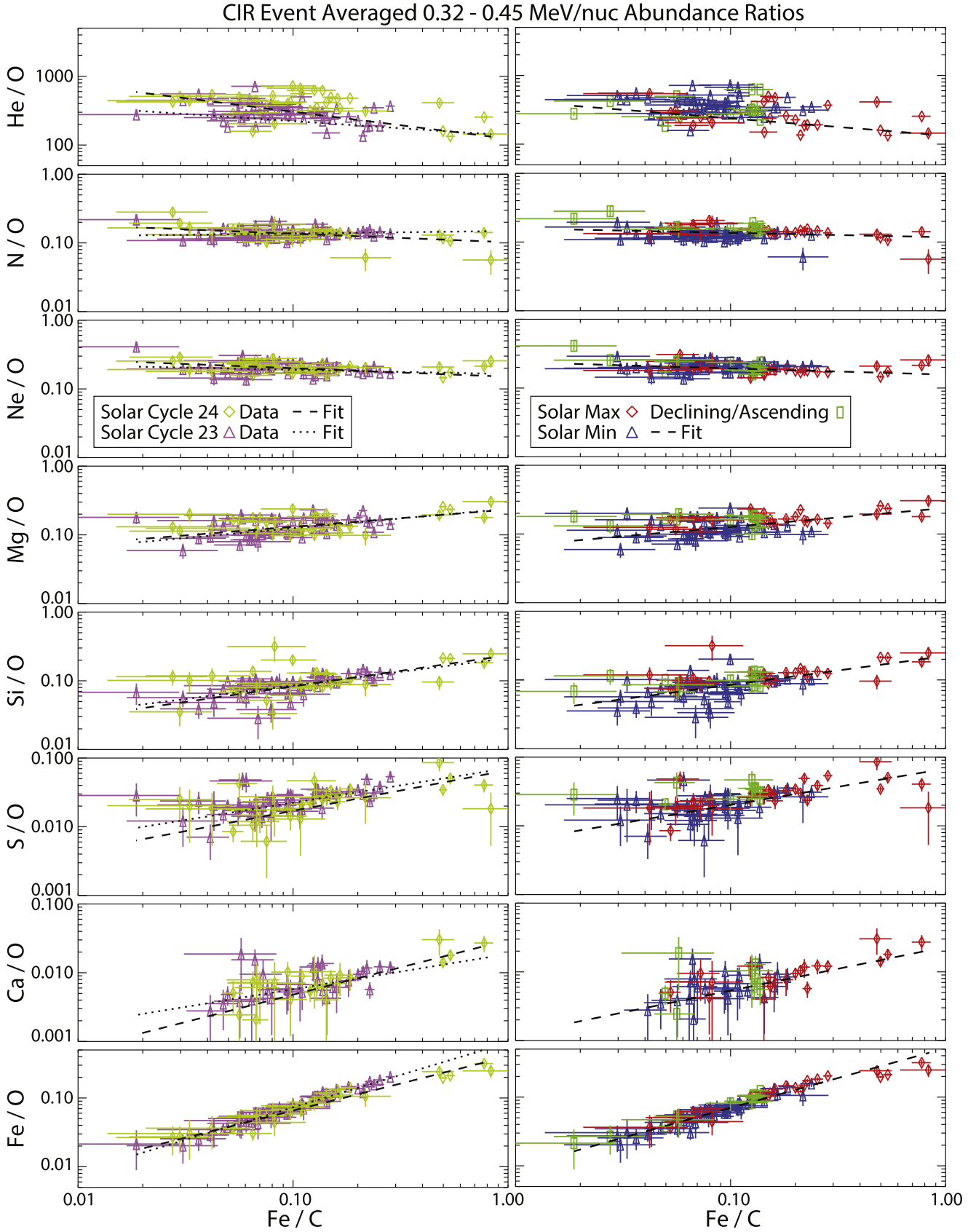

Figure 3. CIR-associated 0.32–0.45 MeV/nuc abundance of elements, ordered by mass, normalized to O vs. Fe/C ratio. The left column shows these ratios separated by solar cycles 23 (purple triangles) and 24 (green diamonds) with dotted and dashed lines illustrating power-law fits for cycles 23 and 24, respectively. The right column separates the ratios by solar cycle phase (see the text for more information), with the dashed line illustrating the power-law fit for all CIR intervals.

4. Conclusions

Using 20 yr (1998–2018) of *ACE* ULEIS data, we have compared the CIR-associated suprathermal ion composition for solar cycles 23 and 24. Our conclusions are summarized as follows:

1. CIR-associated compositional variations were nearly identical during solar cycle 24 as in solar cycle 23.
2. The observed solar cycle variations in CIR-associated 0.32–0.45 MeV/nuc Fe/O previously observed for solar cycle 23 (Mason et al. 2012) were seen to be largely repeated in solar cycle 24 (Figure 1 panel A).
3. A small enhancement in CIR-associated Fe/O during the declining phase was observed for both solar cycles 23 and 24, suggesting the seed populations may be different between the declining and ascending phases, since such an enhancement is not observed during the ascending phase.
4. The CIR-associated Fe/O ratio is found to be correlated with both the event-averaged Fe and O intensities, which are found to have a slight solar cycle dependence (Figures 1(B)–(D)). As such, the processes leading to enhancing the Fe intensities during solar maximum may be preferentially accelerating Fe rather than O.
5. The ratios of relative ion abundances during CIRs are found to be virtually the same for both solar cycles 23 and 24 (Figure 3). For both solar cycles, the abundances were found to be near the fast solar wind abundance, with the exception of He and Ne. The fact that the CIR-associated energetic ion composition for both solar cycles 23 and 24 shares so much in common can point to what is likely to be observed in solar cycle 25.

Upcoming observations from both the *Parker Solar Probe* and *Solar Orbiter* missions will allow for future investigations into CIR-associated energetic ion abundance within 1 au, which may provide additional insight into the seed populations and processes that energize ions into suprathermal ion pool.

The work at JHU/APL was supported by NASA grant NNX17AC05G for support of the *ACE* ULEIS experiment.

ORCID iDs

Robert C. Allen https://orcid.org/0000-0003-2079-5683
George C. Ho https://orcid.org/0000-0003-1093-2066
Glenn M. Mason https://orcid.org/0000-0003-2169-9618

References

Chen, G.-M., Xu, J., Wang, W., & Burns, A. G. 2014, JGRA, 119, 7928
Dayeh, M. A., Desai, M. I., Dwyer, J. R., et al. 2009, ApJ, 693, 1588
Desai, M. I., Mason, G. M., Mazur, J. E., & Dwyer, J. R. 2006, ApJL, 645, L81
Drake, J. F., Cassak, P. A., Shay, M. A., Swisdak, M., & Quataert, E. 2009, ApJL, 700, L16
Ebert, R. W., Dayeh, M. A., & Mason, G. M. 2012, ApJL, 754, L30
Feldman, U., & Widing, K. G. 2002, PhPl, 9, 629
Filwett, R. J., Desai, M. I., Dayeh, M. A., & Broiles, T. W. 2017, ApJ, 838, 23
Glockler, G., Geiss, J., Roelof, E. C., et al. 1994b, JGR, 99, A9
Gloeckler, G., & Geiss, J. 2007, SSRv, 130, 139
Gloeckler, G., Geiss, J., Roelof, E. C., et al. 1994a, ApJL, 230, L191
Gopalswamy, N., Akiyama, S., Yashiro, S., et al. 2014, GeoRL, 41, 2673
Li, G., & Lee, M. A. 2015, ApJ, 810, 82
Li, G., Zank, G. P., & Rice, W. K. M. 2005, JGRA, 110, A06104
Marshall, F. E., & Stone, E. C. 1978, JGR, 83, 3289
Mason, G. M. 2000, AIP Conf. Proc. 528, Acceleration and Transport of Energetic Particles Observed in the Heliosphere: ACE 2000 Symp., ed. R. A. Mewaldt et al. (Melville, NY: AIP), 234
Mason, G. M., Desai, M. I., & Li, G. 2012, ApJL, 748, L31
Mason, G. M., Gold, R. E., Krimigis, S. M., et al. 1998, SSRv, 86, 409
Mason, G. M., Leske, R. A., Desai, M. I., et al. 2008, ApJ, 678, 1458
Mewaldt, R. A., Cohen, C. M. S., Mason, G. M., et al. 2015, Proc. ICRC (The Hague), 030
Mewaldt, R. A., Mason, G. M., & Cohen, C. M. S. 2012, in AIP Conf. Proc. 1500, Space Weather: The Space Radiation Environment, ed. Q. Hu et al. (Melville, NY: AIP), 128
Möbius, E., Morris, D., Popecki, M. A., et al. 2002, GeoRL, 29, 1016
Richardson, I. G. 1985, P&SS, 33, 557
Richardson, I. G. 2018, LRSP, 15, 1
Richardson, I. G., Webb, D. F., Zhang, J., et al. 2006, JGRA, 111, A07S09
Roelof, E. C. 2000, in AIP Conf. Proc. 528, Acceleration and Transport of Energetic Particles Observed in the Helioshpere, ed. R. E. Mewaldt et al. (Melville, NY: AIP), 242
Schwadron, N. A., Fisk, L. A., & Gloeckler, G. 1996, GeoRL, 23, 2871
Smith, E. J., & Wolfe, J. H. 1976, GeoRL, 3, 137
Tsurutani, B. T., & Gonzalez, W. D. 1997, in Magnetic Storms, Geophysical Monographs, Vol. 98, ed. B. T. Tsurutani et al. (Washington, DC: AGU), 77
Tsurutani, B. T., Smith, E. J., Pyle, K. R., & Simpson, J. A. 1982, JGR, 87, 7389
Turner, N. E., Mitchell, E. J., Knipp, D. J., & Emery, B. A. 2006, in Recurrent Magnetic Storms: Corotating Solar Wind Steams, ed. B. Tsurutani et al. (Washington, DC: AGU), 113
Van Hollebeke, M. A. I., et al. 1981, in Conf. Proc. Solar Wind 4, ed. H. Rosenbauer (Garching: Max-Plank-Institute fur Aeronomie), 497
von Steiger, R., Schwadron, N. A., Fisk, L. A., et al. 2000, JGR, 105, 27217
Wurz, P., Bochsler, P., Paquette, J. A., & Ipavich, F. M. 2003, ApJ, 583, 489
Zhao, L., Zhang, M., & Rassoul, H. K. 2016, ApJ, 821, 62
Zhao, L., Zhang, M., & Rassoul, H. K. 2017, ApJ, 836, 31